Composition and Spectral Characteristics of Porcelain-Treated Turquoise

Liying Huang, Quanli Chen, Yan Li, Zuowei Yin, Fengshun Xu, Xinxin Gao, and Yang Du

To meet the ever-increasing demand for high-quality natural turquoise, a novel treatment technique utilizing an inorganic additive appeared in the Chinese market around 2019. Turquoise with this treatment bears a strong resemblance to high-quality natural turquoise, with a fine structure and high surface luster, and is known in the Chinese trade as "porcelain-treated" turquoise. This material was characterized by routine gemological methods, environmental scanning electron microscopy, and spectroscopic methods including infrared, ultraviolet/visible, energy-dispersive X-ray fluorescence, and laser Raman spectroscopy. The infrared and ultraviolet/visible reflectance spectra of porcelain-treated turquoise are difficult to distinguish from untreated turquoise. However, porcelain-treated turquoise can be effectively identified by its surface features in combination with low specific gravity, strong luster, high silica concentration (>8.29 wt.%), high atomic ratio of iron to aluminum (>0.22), and low atomic percentage of phosphorus (<37.5%).

Turquoise is hydrous copper aluminum phosphate with a general chemical formula of $CuAl_6(PO_4)_4(OH)_8 \cdot 4H_2O$. It is widely distributed across localities such as China, Egypt (Mansour, 2014), Chile (Evans and Southward, 1914), the United States (Harbottle and Weigand, 1992; Hedquist 2016), Iran (Beale, 1973; Ovissi et al., 2017), and Mexico (Zalinski, 1907; Weigand et al., 1977). The main Chinese sources are Hubei Province (Chen et al., 2012), Shanxi Province (Luo et al., 2017), the Xinjiang Uyghur Autonomous Region (Liu et al., 2018), Anhui Province (Chen and Qi, 2007), and Henan Province (Zhou and Jiang, 2005). Zhushan County in Hubei is the world's largest commercial source, and material from there usually develops dark iron veins because of its association with phosphate, iron, and copper ores (Tu, 1997).

Turquoise with various colors, fine texture, and moderate hardness has generally been used as carving material. The earliest turquoise artifacts in China were found at the Jiahu site in Wuyang County, Henan Province, and were dated back to 7000–5800 BCE (Yang et al., 2017). Porcelain is a world-renowned Chinese invention that originated from pottery around the middle of the Shang Dynasty in the sixteenth century BCE (Song, 2008). The term "porcelain" is used in China to describe the finest luster of turquoise, and high-quality material with such luster is referred to as "natural porcelain" turquoise (box A). This term was adopted because of the resemblance to the soft, bright, and long-lasting luster of porcelain. The luster of turquoise depends on the structure (density) of the material and the quality of polish.

In Brief

- A novel "porcelain" treatment technique for turquoise produces a color and luster extremely similar to that of high-quality untreated turquoise.
- Treatment with silicate filling may be used on porous or "loose" turquoise.
- Porcelain-treated turquoise can be identified by its surface features and a combination of characteristics such as low specific gravity, strong luster, and high silica content (>8.29 wt.%).

See end of article for About the Authors and Acknowledgments.
Gems & Gemology, Vol. 58, No. 4, pp. 438–457,
http://dx.doi.org/10.5741/GEMS.58.4.438
© 2022 Gemological Institute of America

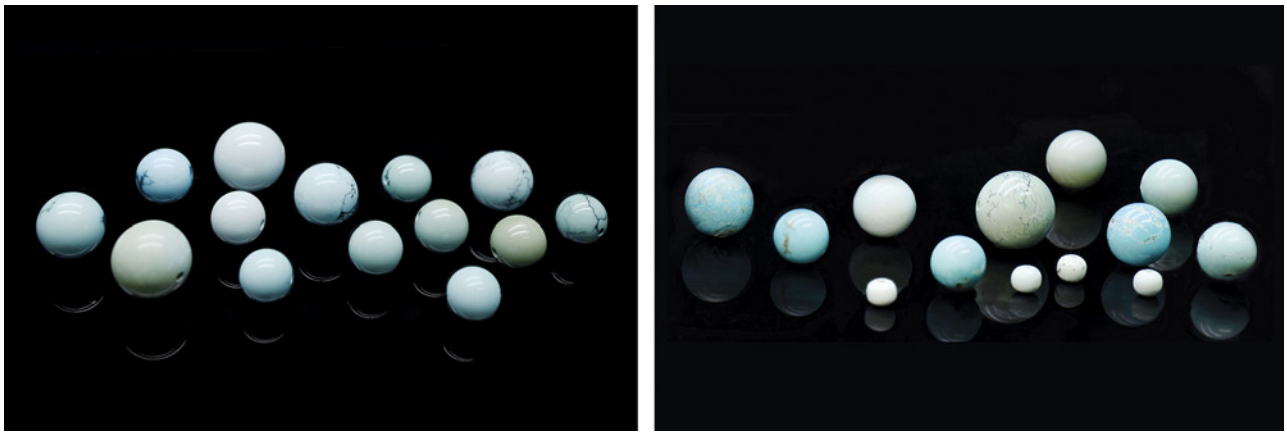

Figure 1. The appearance of natural high-quality turquoise and porcelain-treated turquoise. Left: Natural high-quality turquoise with various colors (the rightmost bead has a diameter of 10.0 mm). Right: Porcelain-treated turquoise with appearance and colors similar to those of natural high-quality turquoise (the smallest bead measures 6.0 × 5.0 mm). Photos by Liying Huang.

In the current Chinese market, natural turquoise is broadly divided into three categories according to density: porcelain, medium-quality, and porous (box A). Porcelain turquoise is sought after for its high luster, uniform color, compact texture, and high hardness. Sky blue porcelain turquoise is regarded as the finest quality. Porous turquoise of low hardness and very light color is regarded as the lowest in quality.

Turquoise is typically a polycrystalline aggregate. Its various colors are attributed to the differences in the type and content of its constituent elements (Luan et al., 2004). Water content and porosity can also affect the color (Foord and Taggart, 1998; Chen, 2009; Liu, 2019). As weathering increases, both crystalline and structural water in turquoise are lost, resulting in a reduction in the structural integrity and a lightening of its color (Chen, 2009). If the space between grain boundaries is small, turquoise usually has low porosity, high density, high hardness, bright color, and strong surface luster. Conversely, if the space between microcrystals is large, the porosity will be high with low hardness (Chen, 2009), which will result in light-colored turquoise with low surface luster. These pores can be filled, to a certain extent, by wax/resin/polymer injection or immersion treatment methods to enhance luster and color. Pore filling not only facilitates turquoise processing but also increases stability and durability (Koivula et al., 1992; McClure et al., 2010; Ou et al., 2016).

In recent decades, the supply of high-quality turquoise has steadily fallen in the Chinese market (Chen, 2009), causing higher prices. Most low- and medium-quality natural turquoise has a light or uneven color, low luster, porous texture, and a tendency to crack (Chen et al., 2010a). These problems make it difficult to meet the ever-increasing consumer demand. Therefore, imitations and "optimized" (treated) products have been on the rise in the world market. Some merchants use other natural gemstone materials to imitate the color of turquoise by dyeing (Xie et al., 2010; Zhu et al., 2016; Schwarzinger and Schwarzinger, 2017), and there are a few synthetic versions available (Choudhary, 2010; Pristacz et al., 2013). However, these are not accepted in the Chinese market.

To enhance the color, texture, and density of low- and medium-quality turquoise, the main method is to inject an organic binder under atmospheric or higher pressures (Koivula et al., 1992; McClure et al., 2010). This process maximizes yield while improving durability. This treatment can be detected by infrared absorption spectroscopy, in which absorption bands are produced by the typical $\nu_s(CH_2)$ symmetrical stretching vibration, $\nu_{as}(CH_2)$ asymmetric stretching vibration, and $\nu(C=C)$ stretching vibration of organic polymers (Xu and Di, 2018).

Surprisingly, a novel technique utilizing an inorganic additive was introduced to the Chinese market in 2019. This method uses an inorganic binder to effectively improve the luster and color of low- and medium-quality material so that it resembles high-quality turquoise (figure 1). The study of this "porcelain-treated" turquoise is relatively new, and there are few reports on the process itself. Only Deng et al. (2019) have studied a specific porcelain treatment and the silicate solution used, in which the molar ratio of the sodium silicate to potassium silicate was 3.5:1.0. Meanwhile, many merchants treat turquoise to raise its price but do not disclose the details of the process. At present, the identification of porcelain-treated

BOX A: CATEGORIES OF TURQUOISE IN THE CHINESE MARKET

Figure A-1. A variety of high-quality "natural porcelain" turquoise products from Hubei Province. A: Sky blue, 56.7 × 35.2 × 24.6 mm, 56.20 g. B: Greenish blue, 32.6 × 25.7 × 10.6 mm, 12.25 g. C: Bluish green, 36.2 × 28.0 × 13.0 mm, 13.92 g. D: Yellowish green, 15.5 × 16.3 × 19.2 mm, 6.5 g. E: Sky blue, 15.9 mm diameter, 5.63 g. F: Greenish blue, 64.7 × 37.5 × 19.2 mm, 48.75 g. Photos by Ren Fei, Jin Yu Turquoise Company.

The turquoise used for "porcelain" treatment is mostly porous, with a loose texture. Silicate filling is used to enhance its color and luster, imitating the appearance of high-quality untreated turquoise. Following this process, the material is called "porcelain-treated" turquoise. The related terms are defined as follows.

"Natural porcelain" turquoise (specific gravity ≥2.70): High-quality turquoise with high density, high hardness (5.5–6.0), bright color, and high surface luster. This material is particularly sought after because its luster resembles porcelain after polishing (figures A-1 and A-2, A and B).

turquoise is challenging, and some labs may mistakenly identify it as untreated. Our investigation found that more than 10% of the turquoise in the Chinese jewelry market is treated with a silicate inorganic binder. Most porcelain-treated turquoise is sold as untreated, which is detrimental to the market.

MATERIALS AND METHODS

Samples. A total of 14 untreated and 26 porcelain-treated samples were examined in this study (table 1). All the samples from Zhushan County were obtained through the long-term cooperation between our research group and miners from the local market. Samples from the Guangzhou jewelry market had no

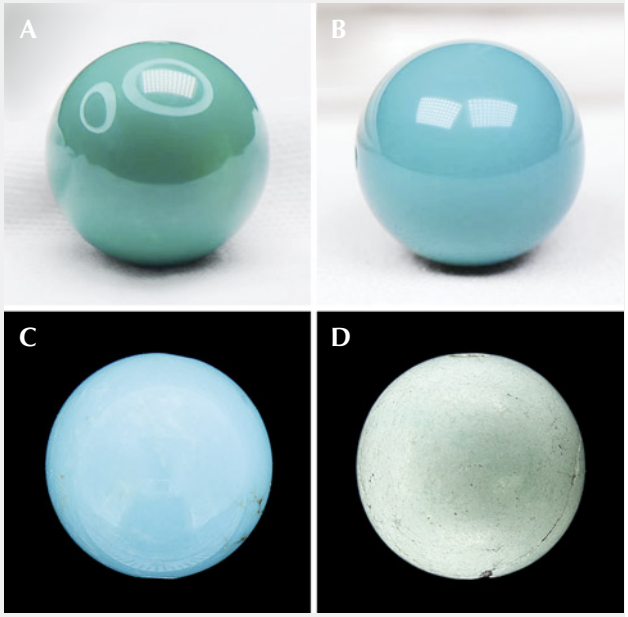

Figure A-2. The appearance of different qualities of natural turquoise. A: Greenish blue "porcelain" turquoise, 14.5 mm diameter, 4.86 g. B: Greenish blue "porcelain" turquoise, 14.5 mm diameter, 4.80 g. C: Medium-quality material, 12.0 mm diameter, 3.80 g. D: Porous material prior to treatment, 10.0 mm diameter, 1.5 g. Photos by Ren Fei, Jin Yu Turquoise Company.

Medium-quality turquoise (SG 2.50–2.70): Density, hardness (4.5–5.5), and color are between "natural porcelain" and porous turquoise, with medium surface luster (between waxy and earthy) (figure A-2, C).

Porous turquoise (SG <2.50): Also known as loose turquoise, with light blue to bluish white color and low surface luster, usually soft or even friable (hardness <4.5). Treatment methods such as the Zachery process (Fritsch et al., 1999), wax injection (Chen, 2009), and dyeing are often used to enhance its appearance (figure A-2, D).

origin record. All 40 specimens were polished (figure 2). To study the internal color distribution and the compositional and structural changes of the porcelain-treated turquoise, five of the samples after treatment were cut in half and polished (figure 3). The specimens were divided into two groups: P (porcelain-treated) and N (natural-color untreated).

The porcelain-treated specimens in this study were sky blue, whitish blue, bluish green, yellowish green, greenish blue, brownish blue, and brownish green. Some displayed an uneven color distribution, and many (such as P4, P5, P8, and N1) had irregular white patches on the surface. All the porcelain-treated samples had a waxy luster (table 1, where H refers to half beads of porcelain-treated turquoise; see also figure 2).

Standard Gemological Testing. Specific gravity (SG) of all specimens was recorded using a hydrostatic balance. Microscopic observations were carried out with a Leica M205A stereo microscope. Both tests were conducted at the Gemmological Institute, China University of Geosciences in Wuhan (GIC).

Infrared Spectroscopy. Infrared spectroscopy analysis was carried out using a Bruker Vertex 80 Fourier-transform infrared spectrometer at GIC. A small amount of sample and KBr powder (weight ratio of 1:150) were mixed, ground, and pressed to make a KBr tablet for transmission spectroscopy. The following conditions were used to test the tablet: 220 V scanning voltage, 6 mm raster, 10 kHz scanning rate, 32 scans, 400–4000 cm^{-1} range, and 4 cm^{-1} resolution. Baseline corrections were made using Bruker's OPUS spectroscopy software.

Ultraviolet/Visible (UV-Vis) Spectroscopy. A UV-Vis spectrophotometer (PerkinElmer Lambda 650 S) was used to test the samples' color characteristics at GIC. The test conditions were as follows: surface reflection method, 1 nm resolution, 100 ms collection time, a deuterium lamp excitation source at a color temperature of 2850 K, and a wavelength range of 250–800 nm.

Energy-Dispersive X-Ray Fluorescence (EDXRF) Spectroscopy. Chemical composition was determined by energy-dispersive X-ray fluorescence using a ThermoFisher ARL Quant'x EDXRF analyzer equipped with a rhodium-palladium X-ray tube and a Peltier-cooled detector at GIC. The analyses were performed using a voltage of 0 to 50 kV, a current of 1.98 mA, and a spot size of 1.5 mm^2. Testing was carried out based on the turquoise working curve established by Liu and Yang (2018). The details of the turquoise working procedures were established as follows: Liu and Yang (2018) conducted laser ablation–inductively coupled plasma–mass spectrometry

TABLE 1. Characteristics of turquoise samples from this study.

Group	Sample	Color	Shape	Luster	SG	Weight (g)	Market Source
Porcelain-treated	P1	Whitish blue	Drilled bead	Waxy	1.95	0.190	Zhushan
	P2	Sky blue	Drilled bead	Waxy	2.35	1.662	Guangzhou
	P3	Whitish blue	Drilled bead	Waxy	2.14	3.094	Guangzhou
	P4	Sky blue	Drilled barrel	Waxy	2.39	4.006	Guangzhou
	P5	Sky blue	Drilled bead	Waxy	2.44	5.249	Guangzhou
	P6	Greenish blue	Drilled bead	Waxy	2.33	2.190	Zhushan
	P7	Bluish green	Drilled bead	Waxy	2.47	2.538	Zhushan
	P8	Sky blue	Drilled bead	Waxy	2.63	2.922	Zhushan
	P9	Whitish blue	Drilled bead	Waxy	1.92	2.074	Guangzhou
	P10	Green-blue	Drilled bead	Waxy	1.93	2.129	Zhushan
	P11	Whitish blue	Drilled bead	Waxy	1.92	0.175	Zhushan
	P12	Whitish blue	Drilled bead	Waxy	1.89	0.203	Zhushan
	P13	Brownish blue	Drilled bead	Waxy	2.38	2.075	Guangzhou
	P14	Sky blue	Drilled bead	Waxy	2.41	2.051	Guangzhou
	P15	Sky blue	Drilled bead	Waxy	2.56	1.957	Guangzhou
	P16	Whitish blue	Drilled bead	Waxy	1.94	1.085	Zhushan
	P17	Whitish blue	Drilled bead	Waxy	2.13	1.000	Zhushan
	P18	Yellowish green	Drilled bead	Waxy	2.55	4.485	Guangzhou
	P19	Sky blue	Drilled bead	Waxy	2.45	1.385	Guangzhou
	P20	Whitish blue	Drilled bead	Waxy	2.13	2.191	Guangzhou
	P21	Brownish green	Drilled bead	Waxy	2.36	5.296	Guangzhou
	H1	Whitish blue	Half bead	Waxy	2.15	0.059	Zhushan
	H2	Sky blue	Half bead	Waxy	2.33	1.100	Guangzhou
	H3	Whitish blue	Half bead	Waxy	2.38	0.344	Zhushan
	H4	Yellowish green	Half bead	Waxy	2.39	1.236	Guangzhou
	H5	Sky blue	Half bead	Waxy	2.41	1.792	Zhushan
Untreated	N1	Whitish blue	Block	Waxy	2.48	3.355	Guangzhou
	N2	Yellowish green	Block	Waxy	2.66	1.002	Zhushan
	N3	Whitish blue	Drilled barrel	Waxy	2.35	1.239	Zhushan
	N4	Sky blue	Block	Weak porcelain	2.68	3.518	Zhushan
	N5	Greenish blue	Drilled barrel	Weak porcelain	2.69	6.647	Zhushan
	N6	Whitish blue	Drilled bead	Earthy	2.50	1.683	Zhushan
	N7	Sky blue	Block	Waxy	2.64	3.029	Zhushan
	N8	Greenish blue	Block	Waxy	2.65	0.713	Zhushan
	N9	Greenish blue	Block	Waxy	2.58	2.128	Zhushan
	N10	Sky blue	Drilled bead	Waxy	2.61	1.301	Zhushan
	N11	Whitish blue	Drilled bead	Waxy	2.56	1.373	Zhushan
	N12	Whitish blue	Block	Earthy	2.58	0.830	Zhushan
	N13	Whitish blue	Drilled barrel	Earthy	2.60	0.880	Zhushan
	N14	Whitish blue	Block	Earthy	2.49	0.581	Zhushan

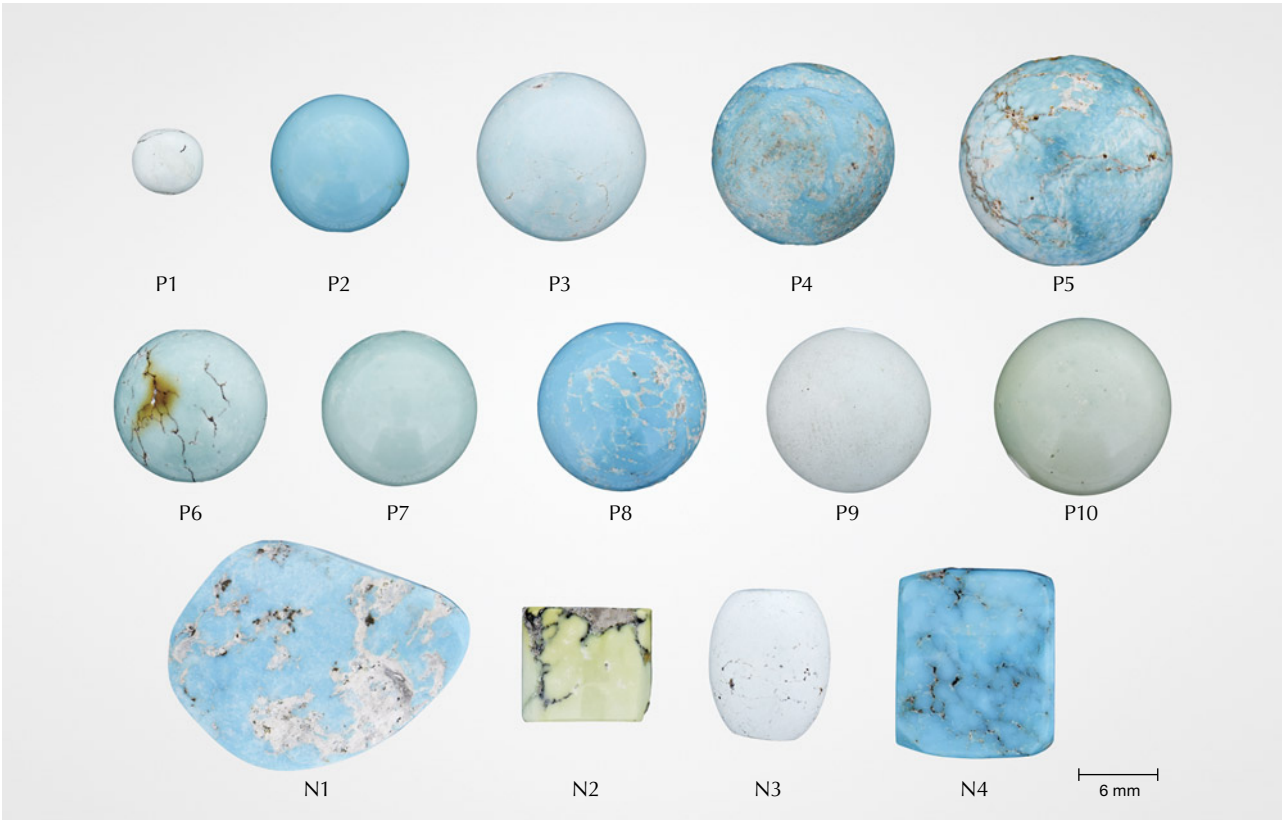

Figure 2. Ten of the porcelain-treated turquoise samples (P1–P10) and four of the untreated specimens (N1–N4) characterized in this study. Photos by Liying Huang.

(LA-ICP-MS) testing on a different set of 26 pieces of untreated turquoise from Zhushan, nine uniform color test positions were selected for each sample, and the average value was taken as the standard value of each sample. Twenty-one of 26 turquoise samples with a composition gradient were selected as reference standards, and the working curve of analytical elements was established. Ten elements (aluminum, silicon, phosphorus, potassium, calcium, copper, iron, vanadium, chromium, and zinc) were selected for examination.

Raman Spectroscopy. A Raman spectrometer (Bruker Senterra R200L) was used to explore the abnormally high SiO_2 content in the porcelain-treated turquoise at GIC. The laser wavelength was 532 nm, the laser power was 20 mW, and the acquisition time was 30 s. The laser spot size was 50 µm, the resolution was 9–15 cm^{-1}, and the test range was 34–1500 cm^{-1}.

Environmental Scanning Electron Microscope (ESEM). A Quanta 200 environmental scanning electron microscope was used to observe the structural

Figure 3. Porcelain-treated turquoise samples in group P that were cut in half for internal studies (red points indicate EDXRF testing locations). Photos by Liying Huang.

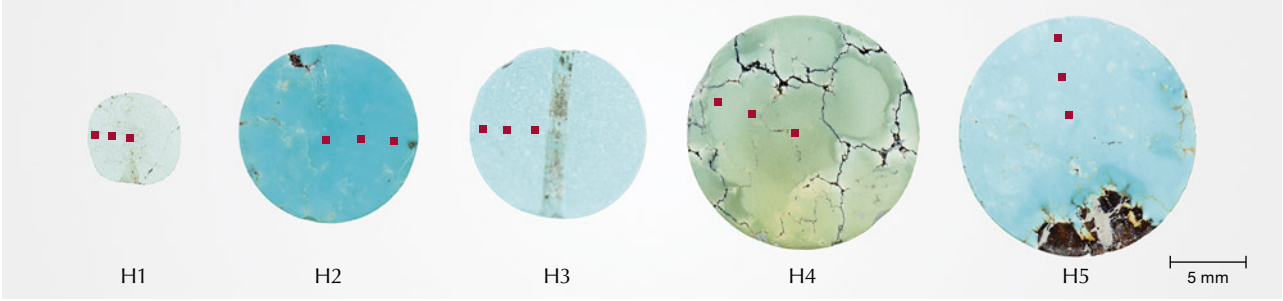

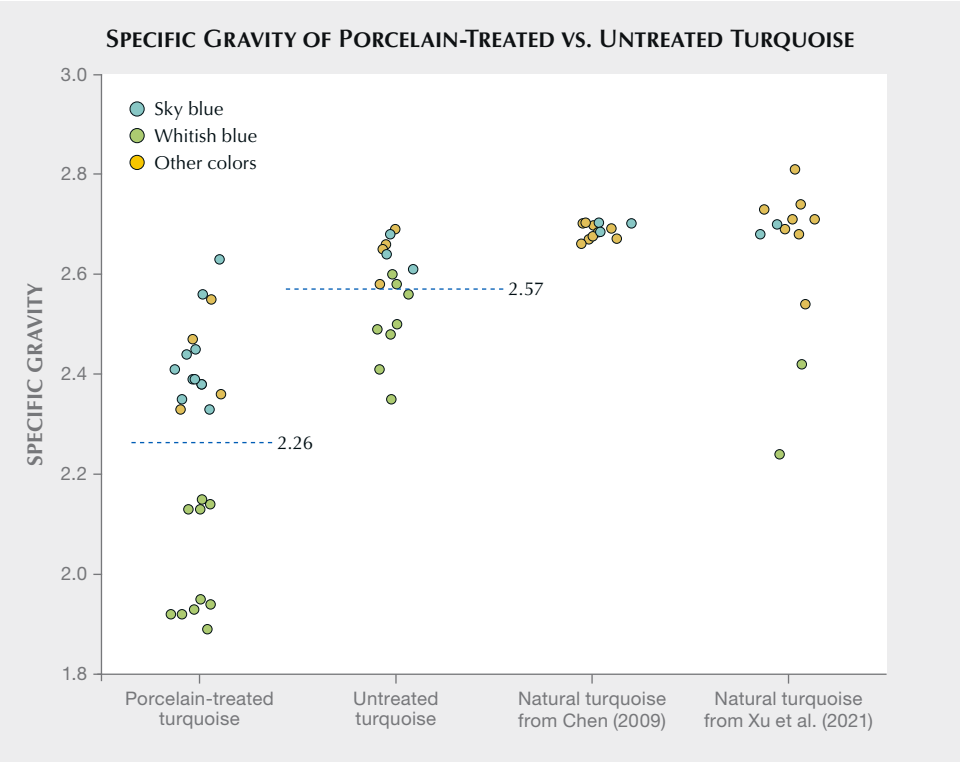

Figure 4. SG values of the samples from the present study and from Chen (2009) and Xu et al. (2021), two studies that examined many different qualities of untreated turquoise found in China. Dashed lines represent the average SG value of porcelain-treated turquoise (2.26) and untreated turquoise (2.57) in our study.

characteristics of the porcelain-treated specimens at the State Key Laboratory of Geological Process and Mineral Resources, China University of Geosciences in Wuhan (CUG). The test conditions were as follows: room temperature of 15° to 20°C, a relative humidity of <80%, an acceleration voltage of 20 kV, and a magnification of 7× to 10^6×. Secondary electron images were collected. Three porcelain-treated samples (P4, H2, and H3) and one untreated turquoise sample (N14) were selected to obtain cross sections of polished areas coated with 10–20 nm of gold using SEM.

RESULTS AND DISCUSSION

Gemological Properties. All the porcelain-treated and untreated turquoise samples were tested for their standard gemological properties.

Specific Gravity. Turquoise is a polycrystalline aggregate, and its surface pores easily absorb water. Therefore, specific gravity (table 1) should be recorded within 2 seconds after immersion (He et al., 2018). The SG of the untreated samples ranged from 2.35 to 2.69, with an average of 2.57. There was a limited number of untreated turquoise samples in the test set, and previous studies have shown that the SG of untreated turquoise with a poor texture is typically less than 2.50, while turquoise with a high-quality texture generally has an SG greater than 2.70 (Chen, 2009; Xu et al., 2021).

The SG of the porcelain-treated specimens ranged from 1.89 to 2.56, with an average of 2.26 (figure 4). The porcelain-treated whitish blue samples' SG range was 1.89–2.38 (average of 2.05), while the untreated whitish blue samples' range was 2.35–2.61 (average of 2.51). The porcelain-treated sky blue samples' SG range was 2.33–2.63 (average of 2.44), while the untreated sky blue samples' range was 2.62–2.68 (average of 2.65). Untreated sample data from Chen (2009) and Xu et al. (2021) are also in this range. As can be seen, the average SG of porcelain-treated turquoise (both whitish blue and sky blue) was lower than the average SG of untreated turquoise.

The luster and hardness of untreated turquoise are related to its density (Wang, 1986; Foord and Taggart, 1998). The denser the structure and the higher the hardness, the stronger the luster. Untreated porcelain turquoise shows a strong waxy to glassy luster after polishing, while porous material has an earthy to weak waxy luster. The porcelain-treated specimens in this study generally had a higher luster (waxy to weak porcelain). Their density was similar to that of low-quality turquoise typically chosen for treatment. Hence, the combined characteristics of low density and strong surface luster can be used to identify porcelain-treated material.

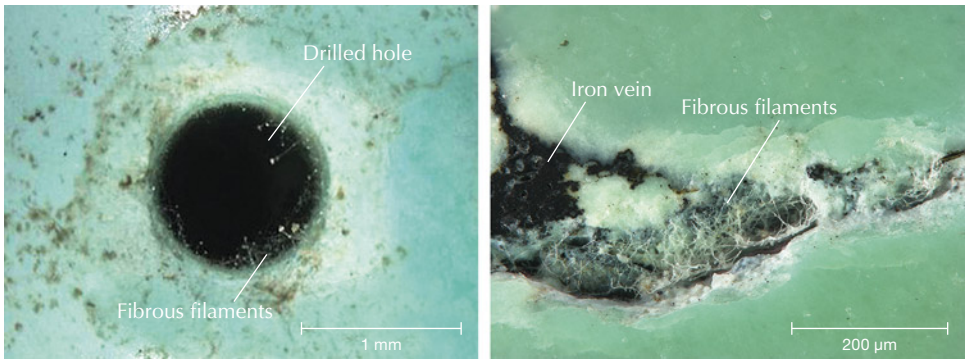

Figure 5. Surface characteristics of porcelain-treated samples P1 and P10. Left: Fibrous filaments at the edge of a drilled hole on P1. Right: Fibrous filaments near the depression of an iron vein on P10. Photomicrographs by Liying Huang.

Morphological Characteristics. Most of the porcelain-treated specimens purchased at the Zhushan market were whitish blue. They had waxy luster and a uniform color distribution, such as sample P1 in figure 2. The porcelain-treated turquoise specimens purchased in the Guangzhou market had various colors, including sky blue, whitish blue, and yellowish green. Some of the samples from both markets had high color saturation and waxy luster, such as samples P2–P10 in table 1.

Microscopic examination of porcelain-treated specimens P1, P5, and P10 showed obvious granular transparent crystals and fibrous filaments at pore channels and near the depressions of iron lines (figure 5). Specimen P1 originally had a waxy luster, but one week in an ambient environment (humidity above 50%) dulled its luster (figure 6, left) and left a blue spot on the surface (figure 6, right). Specimen H4 had a nonuniform color distribution with deep color along the edge and a bleached appearance along the iron vein. We attributed this uneven distribution to immersion in the filling material during treatment (figure 7, left). A round, transparent blob of melt with a greasy luster appeared on the surface of specimen P10 (figure 7, right).

Magnification and SG testing revealed that the stability of porcelain-treated turquoise is related to the density of the rough material before enhancement. Higher density produces a more stable color and luster. Because turquoise with high density is less porous, the filling material does not easily come out of the pores and the treatment is relatively stable.

Chemical Composition Analysis. All the porcelain-treated samples (P1–P21 and H1–H5) and ten of the untreated specimens with good luster (N1–N5 and N7–N11) were measured for major elements with EDXRF. All the porcelain-treated turquoise and some untreated samples (N1–N4) were also analyzed by Raman spectroscopy. Two or three different locations with uniform color were selected for each specimen, and each test location was tested twice with the av-

Figure 6. Surface characteristics of porcelain-treated turquoise sample P1. Left: After one week in a humid atmosphere, the surface changed from waxy in luster and uniform in color to an earthy luster with brown spots. Right: A blue spot also appeared on the surface of sample P1 after one week in an unstable ambient atmosphere. Photos by Liying Huang.

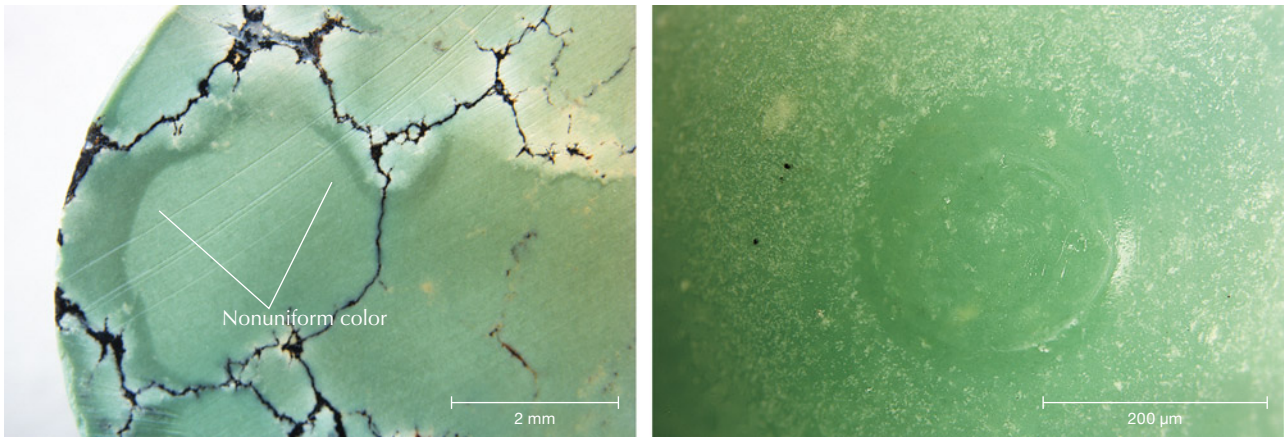

Figure 7. Surface characteristics of porcelain-treated turquoise samples H4 and P10, respectively. Left: H4 had a nonuniform color distribution, with deep color along the edge and a bleached look along an iron vein. Right: A round, transparent spot of melt with a greasy appearance on the surface of sample P10. Photos by Liying Huang.

erage value reported with detection limits in table 2. The main chemical compositions of the porcelain-treated and untreated turquoise were similar, composed mainly of CuO, Al_2O_3, and P_2O_5, with traces of FeO_T (including Fe_2O_3 and FeO), ZnO, SiO_2, K_2O, and CaO. Turquoise's ideal chemical formula is $CuAl_6(PO_4)_4(OH)_8 \cdot 4H_2O$, in which iron can replace some of the aluminum and zinc can replace copper (Zhang et al., 1984; Foord and Taggart, 1998; Chen, 2009; Liu, 2019). The ideal formula in weight percentage of oxides was 37.60% Al_2O_3, 34.90% P_2O_5, 9.78% CuO, and 17.72% H_2O. The original EDXRF test results do not include water (the total oxide content is approximately 100%), so we accounted for water by multiplying by 0.8228 (100% minus the 17.72% attributable to water). The results of these calculations are presented in table 2 (note the approximately 82% total for all of the measured samples) and plotted in figure 8. Figure 8 plots the differences between the major elements of porcelain-treated and

TABLE 2. Element concentrations (in wt.%) in porcelain-treated and untreated turquoise, measured by EDXRF.

Oxide	Porcelain-treated min–max (avg.)	Untreated min–max (avg.)	Untreated sample N2 min–max (avg.)	Ideal turquoise	Average detection limit (wt.%)
Al_2O_3	14.75–28.49 (23.78)	22.65–32.62 (29.51)	30.72–31.16 (30.93)	37.60	0.16
P_2O_5	22.03–34.18 (29.81)	31.44–38.22 (35.73)	35.82–36.17 (36.04)	34.90	0.12
CuO	7.16–11.37 (9.19)	0.82–11.38 (7.06)	0.82–0.88 (0.85)	9.78	0.0038
FeO_T	1.12–16.95 (4.14)	0.29–14.42 (4.00)	0.94–0.95 (0.95)	—	0.0042
ZnO	0.00–1.29 (0.17)	0.11–10.28 (2.47)	9.78–10.28 (10.02)	—	0.014
SiO_2	8.30–29.45 (14.15)	1.11–8.01 (2.57)	2.50–2.84 (2.71)	—	0.33
K_2O	0.03–0.94 (0.14)	0.06–0.26 (0.11)	0.06–0.08 (0.07)	—	0.0061
CaO	0.02–0.64 (0.19)	0.05–0.93 (0.18)	0.05–0.08 (0.06)	—	0.0047
H_2O	na[a]	na	na	17.72	—
Total[b]	81.57	81.63	81.63	100	—

[a] *na = not analyzed*
[b] *The given totals were added up from the average wt.% of the porcelain-treated and untreated turquoise, which did not include the content of H_2O.*

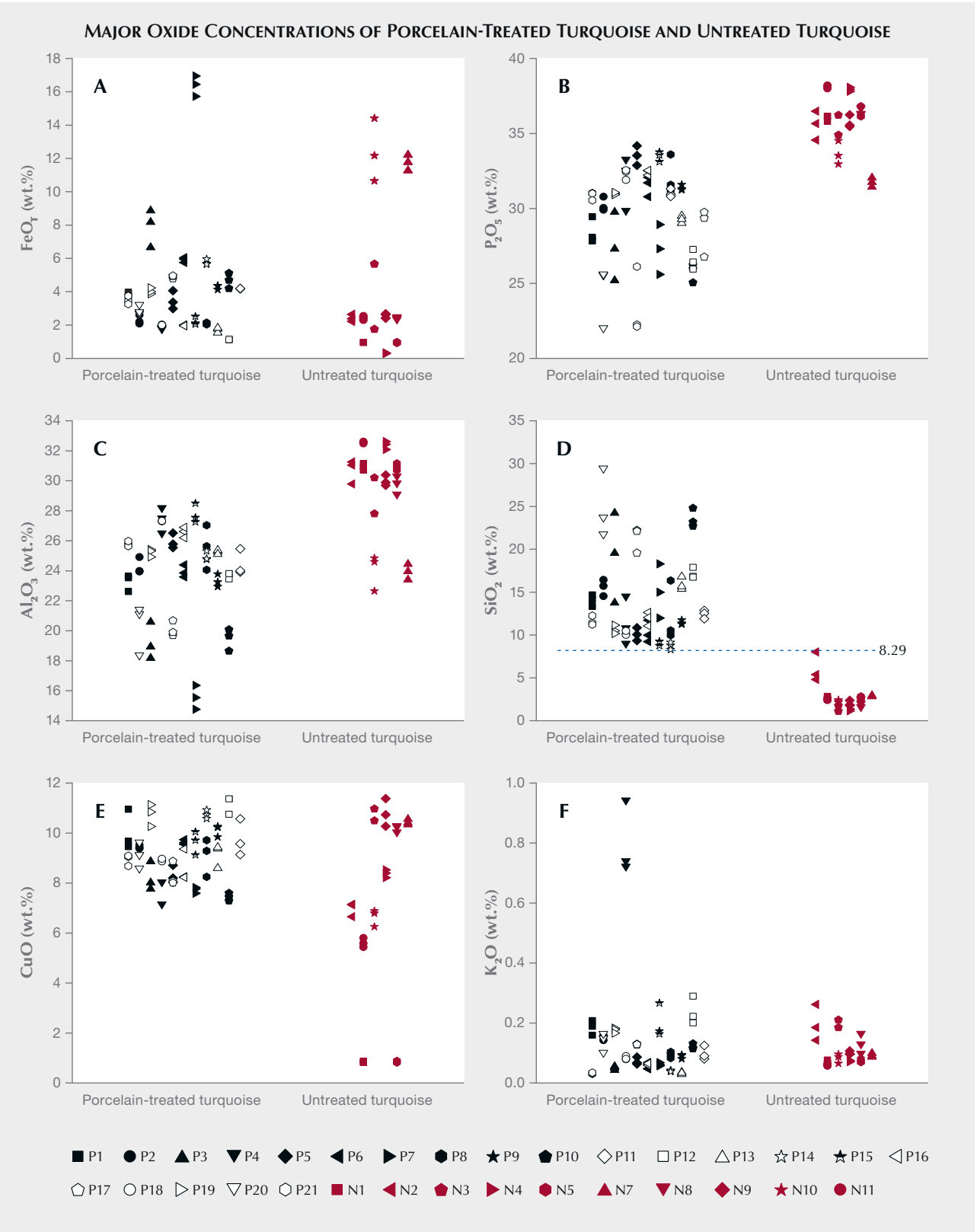

Figure 8. A–F: Major oxide concentrations corrected for water of porcelain-treated turquoise (black) and untreated turquoise (red). The different shapes represent different specimens (P1–P21, N1–N5, and N7–N11), while the blue line in the SiO_2 plot is the minimum value of the SiO_2 content of porcelain-treated turquoise.

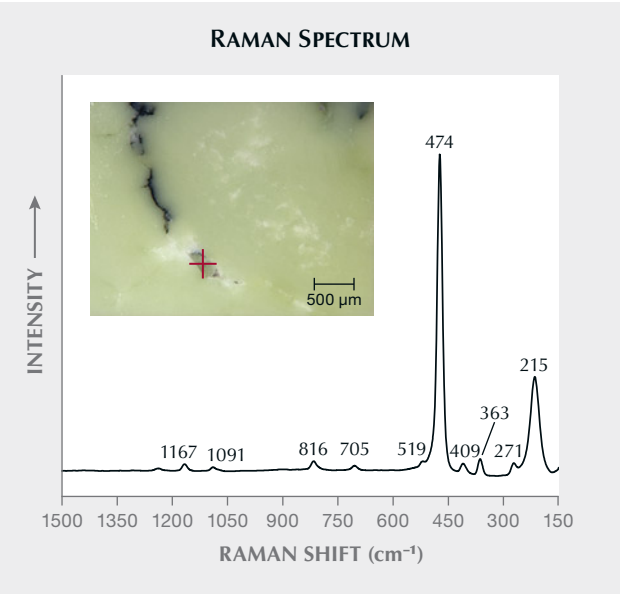

Figure 9. The Raman spectrum of quartz in untreated turquoise specimen N2.

natural turquoise. Among them, sample N2 had a ZnO to CuO weight percentage ratio greater than 1.0, making it a copper-zinc turquoise (Foord and Taggart, 1998).

The silica concentrations of all of the porcelain-treated samples were above 8.29 wt.%, generally higher than that of untreated turquoise. The silica contents of all the untreated samples tested in this study were all lower than 8.29 wt.% (the silica content of most untreated turquoise is <3 wt.%) (figure 8). Occasionally, the silica content of untreated turquoise can be high due to the existence of associated minerals, such as quartz and some clay minerals. In those cases, the elevated silica content was caused by associated minerals, according to the Raman spectroscopy results (figure 9). It was inferred that the binder used in the porcelain treatment contained silicon.

The weight percentages of aluminum + iron, copper + zinc, and phosphorus were converted into atomic percentages and plotted as the vertices of a ternary diagram (figure 10). It can be seen that untreated and porcelain-treated turquoise occupy two different areas, with some overlap. The atomic percentage of phosphorus in untreated turquoise is generally greater than 37.5%, significantly higher on average than in porcelain-treated turquoise. Data of untreated turquoise from Xu et al. (2021) are in agreement with our findings (blue points in figure 10). Therefore, the relationships between aluminum + iron, copper + zinc, and phosphorus are a useful

Figure 10. Left: Ternary diagram showing the composition of untreated (including data from Xu et al., 2021) and porcelain-treated turquoise in terms of copper + zinc, aluminum + iron, and phosphorus. Right: A partial enlargement of the ternary diagram. The atomic percentage of phosphorus in untreated turquoise is generally greater than 37.5%, significantly higher on average than in porcelain-treated turquoise.

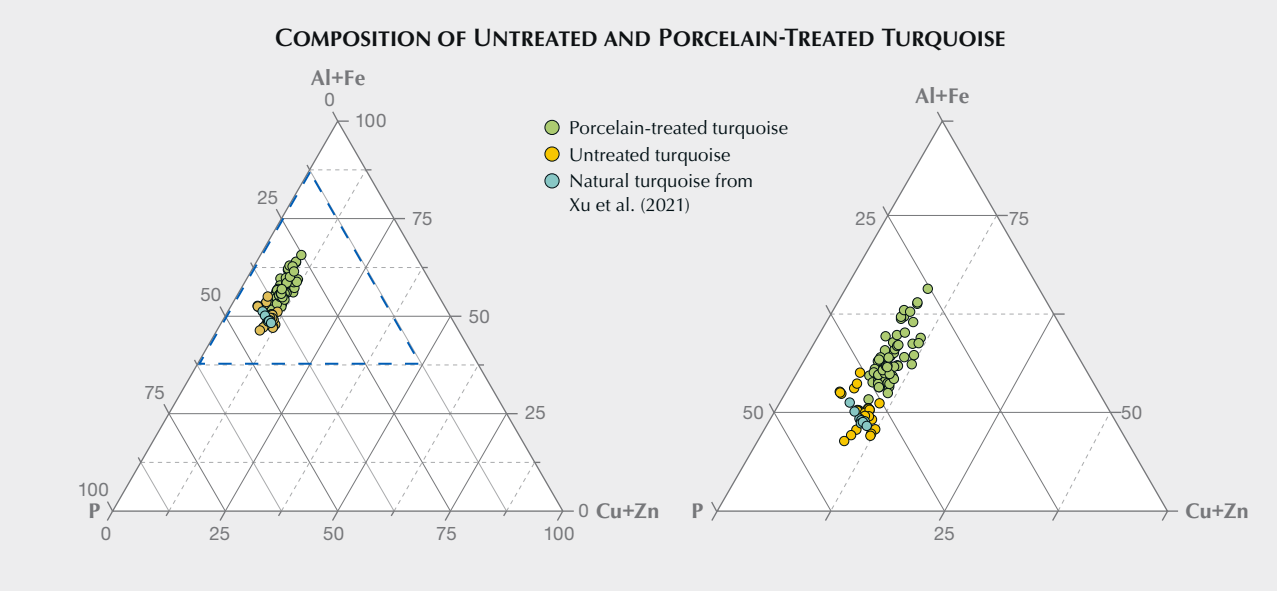

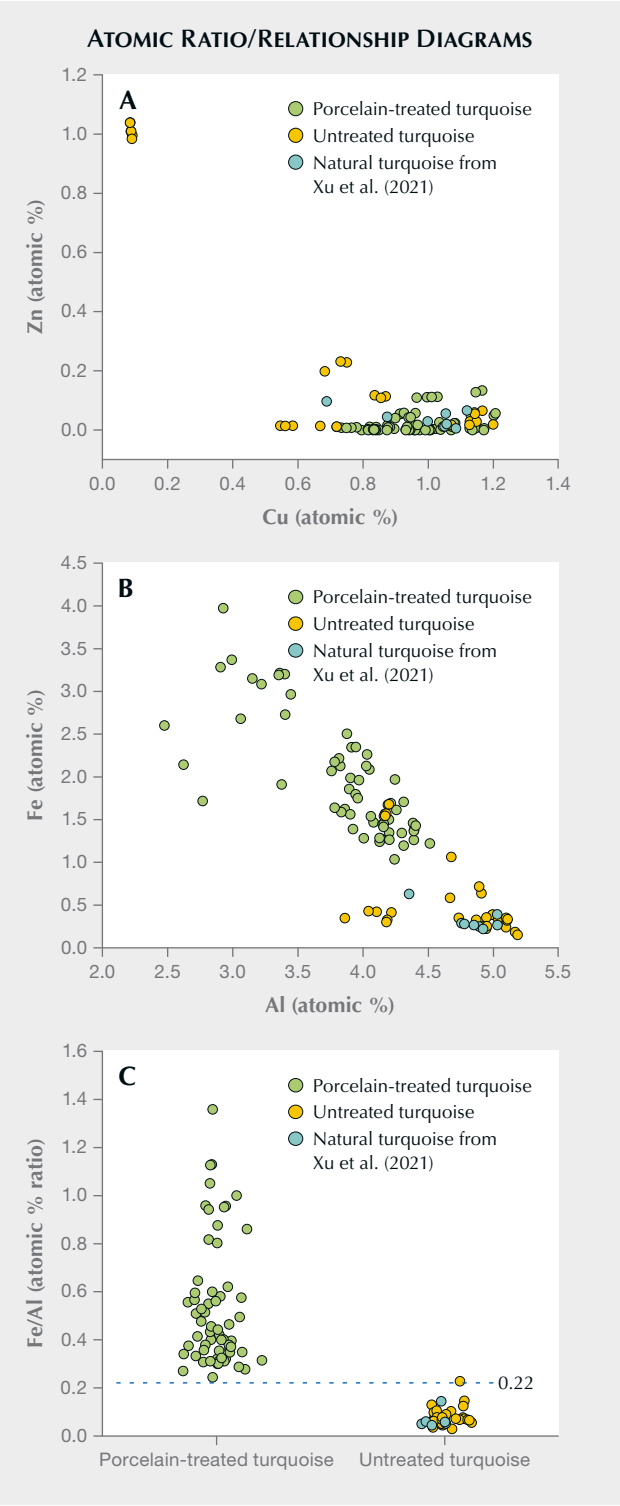

Figure 11. Diagrams showing the relationship between copper vs. zinc (A) and aluminum vs. iron (B) in atomic percentage. C: Atomic ratio of iron and aluminum scatter diagram, in which the dashed line is the boundary value of Fe/Al ratio between porcelain-treated and natural turquoise (0.22). The Fe/Al ratio of porcelain-treated turquoise is higher.

means of separation. In addition, two-dimensional separation plots were generated between zinc and copper and between iron and aluminum (figure 11, A and B). It is impossible to distinguish porcelain-treated turquoise through the content relationship of zinc and copper. Figure 11 (B and C) shows some separation between untreated and porcelain-treated turquoise. Because the Fe/Al ratio of porcelain-treated turquoise (>0.22) is higher than that of untreated turquoise, it can potentially be distinguished by its iron/aluminum ratio.

Among the tested samples, the silica content of untreated specimen N2 was as high as 8 wt.%. Microscopic observation found a light-colored mineral with a transparent glassy luster, which was identified as quartz by Raman analysis (figure 9). The Raman shifts of 1091 and 816 cm^{-1} were caused by asymmetric and symmetrical stretching vibrations of Si-O-Si, and the peak values were low. The bending vibration Raman shift of Si-O-Si was 474 cm^{-1}, and its peak was the highest. All the characteristic scattering peaks were sharp, and the full width at half maximum was small, indicating high crystallinity (Krishnan, 1945; Krishnamurti, 1958). Comparing the Raman spectra of untreated and porcelain-treated turquoise, there is little difference in spectral peaks from previous studies (Čejka et al., 2015; Štubňa and Andrášiová, 2021) (figure 12). In the 2800–3000 cm^{-1} range, some porcelain-treated material exhibited a weak peak, while untreated turquoise did not. The peak at the position of 2800–3000 cm^{-1} may be attributed to the asymmetrical stretching vibration and stretching vibration of CH_2 (Chen et al., 2010b). This peak often occurs in turquoise treated with an organic binder. This peak from porcelain-treated turquoise at the position of 2800–3000 cm^{-1} (figure 12) is weak due to low spectral resolution, so the material cannot be identified as porcelain-treated from this peak. Since the EDXRF test found a high concentration of silicon in the porcelain-treated turquoise, it was inferred that the fillings are inorganic (containing silicate).

To explore whether the high silica content is caused by the porcelain treatment, three test positions of equal distance from the edge to the center of the split samples in group P (figure 3) were measured with EDXRF. Each different test location was tested twice and averaged. The silica content near the edge was higher than that at the center, indicating that the high silica content of the porcelain-treated turquoise was due to the enhancement process (figure 13) and the observed variations from sample to sample were caused by the silicon-containing filling.

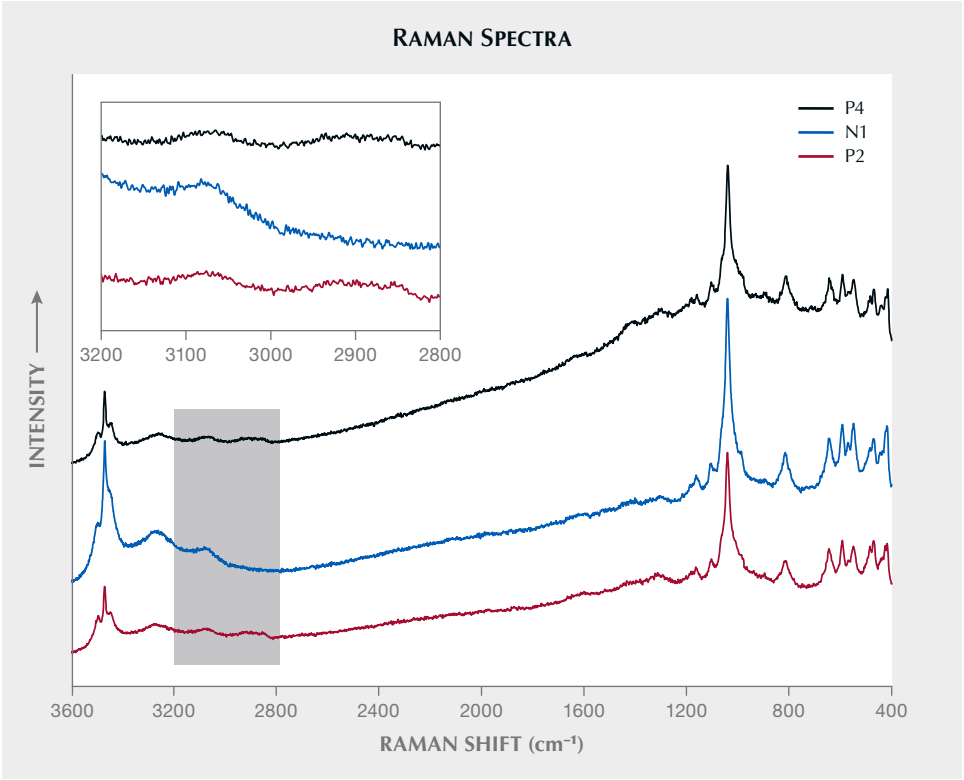

Figure 12. Raman spectroscopy of untreated (N1) and porcelain-treated (P2, P4) turquoise. The Raman spectrum characteristics of the treated and untreated turquoise are consistent. Inset: The close-up of the 2800–3200 cm^{-1} range shows that porcelain-treated (P2, P4) turquoise has a broad and weak absorption band around 2850–2950 cm^{-1}, while untreated turquoise does not. Spectra are offset vertically for clarity.

Infrared Spectroscopy Features. All the porcelain-treated and untreated turquoise specimens were measured with infrared spectroscopy. The obtained infrared absorption spectra were divided into two regions: 4000–1300 cm^{-1} (region I) and 1300–400 cm^{-1} (region II). In the ideal turquoise structure, group theory analysis shows that there are two PO_4^{3-} units in nonequivalent positions, two H_2O units in nonequivalent positions, and four OH units in nonequivalent positions. Different units have different vibration characteristics. The vibration modes and frequencies of OH, H_2O, and PO_4^{3-} units determine the infrared absorption spectra of turquoise (Lind et al., 1983; Fritsch and Stockton, 1987; Chen, 2009; Čejka et al., 2015).

Figure 13. Distribution of silica in three different locations in the porcelain-treated specimens (H1–H5) based on EDXRF results. From the edge position to the center position, the samples show different degrees of silica concentration decrease.

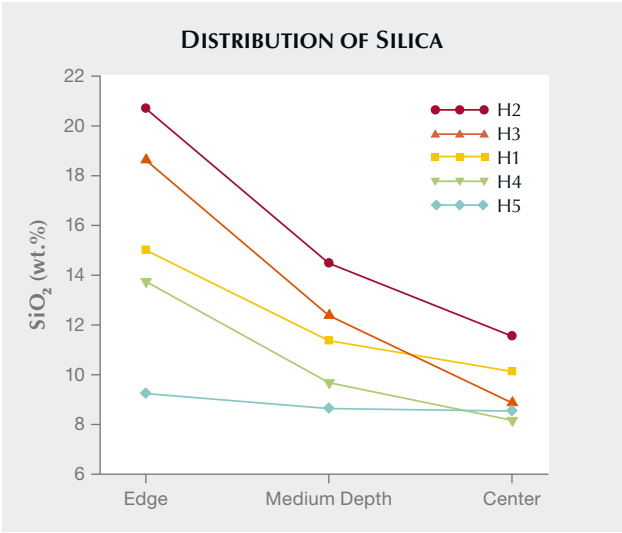

Untreated Turquoise. The absorption characteristics of untreated turquoise in region I were consistent with previous research (Chen et al., 2007). The absorption near 3500–3400 cm^{-1} corresponds to the ν(OH) stretching vibration, the absorption near 3300–3000 cm^{-1} is a δ(H_2O) stretching vibration, and the peak near 1640 cm^{-1} is the δ(H_2O) bending vibration (figure 14, left).

Untreated turquoise showed four vibration mode frequencies of PO_4^{3-} in region II. The 1200–1000 cm^{-1} asymmetric stretching vibration absorption peak was $\nu_3(PO_4^{3-})$, the four-fold set of peaks with strong absorbance. There was a $\nu_1(PO_4^{3-})$ symmetrical stretching vibration frequency near 900 cm^{-1}, with weak absorption. A δ(OH) out-of-plane bending vibration frequency was located near 840 and 786 cm^{-1}. The

bending vibration frequency of $\nu_4(PO_4^{3-})$ was near 646, 595, 549, and 476 cm^{-1}, and a symmetrical bending vibration frequency of $\nu_2(PO_4^{3-})$ was near 470–410 cm^{-1} with weak absorption. Its main peak was near 1100 cm^{-1} (figure 14, left).

Porcelain-Treated Turquoise. The porcelain-treated turquoise in region I showed an absorption peak caused by the stretching vibration of ν(OH) near 3511 and 3465 cm^{-1}, an absorption peak caused by the stretching vibration of $\nu(H_2O)$ near 3300 and 3087 cm^{-1}, and an absorption peak caused by the bending vibration of $\delta(H_2O)$ near 1640 cm^{-1} (figure 14, right). Those absorption peaks were basically the same as those of untreated turquoise (Farmer, 1974).

The infrared absorption spectroscopy characteristics of porcelain-treated turquoise in region II showed that 1160, 1108, 1060, and 1020 cm^{-1} were the asymmetric stretching vibration absorption peaks of $\nu_3(PO_4^{3-})$ (figure 14, right). The symmetrical stretching vibration frequency of $\nu_1(PO_4^{3-})$ was near 900 cm^{-1}, the out-of-plane bending vibration frequency of δ(OH) was located at 840 and 786 cm^{-1}, and the bending vibration frequency of $\nu_4(PO_4^{3-})$ was near 649, 609, 580, and 476 cm^{-1}. The symmetrical bending vibration frequency of $\nu_2(PO_4^{3-})$ was located near 470–410 cm^{-1}; its absorption was weak, and some samples did not show this peak. The main peak of most samples was 1108 cm^{-1}, consistent with that of the untreated specimens.

According to Farmer (1974), the absorption peak caused by the ν(Si-O-Si) stretching vibration was near 1100–1000 cm^{-1} with strong absorption. The ν(Si-O-Si) asymmetric stretching vibration frequency was near 1089 cm^{-1} with strong absorption. The ν(Si-O-Si) symmetric telescopic vibration frequency splits at 800 and 781 cm^{-1}, and the asymmetric and symmetrical variable angle vibrations were located at 696 and 464 cm^{-1}, respectively. The asymmetric stretching vibration of phosphate $\nu_3(PO_4^{3-})$ was located at the strong absorption of 1100–1050 cm^{-1}, and the symmetrical stretching vibration of $\nu_1(PO_4^{3-})$ was located at 970 cm^{-1}, which is very weak. A weak bending vibration of $\nu_4(PO_4^{3-})$ was located at the absorption wavelength of 630–540 cm^{-1}, and a weak symmetrical bending vibration of $\nu_2(PO_4^{3-})$ was located at the absorption wavelength of 470–410 cm^{-1} (Farmer, 1974).

The absorption peak of the ν(Si-O-Si) asymmetric stretching vibration was similar to that of the $\nu_3(PO_4^{3-})$ asymmetric stretching vibration, the absorption peak of the ν(Si-O-Si) symmetrical stretching vibration was similar to that of the δ(OH) out-of-plane bending vibration, and the ν(Si-O-Si) symmetrical stretching vibration absorption peak was close to that of the $\nu_4(PO_4^{3-})$ bending vibration

Figure 14. Left: Infrared absorption spectra of untreated turquoise (N2–N5). Right: Porcelain-treated specimens (P1–P5). The FTIR characteristics of the two groups are consistent. Spectra are offset vertically for clarity.

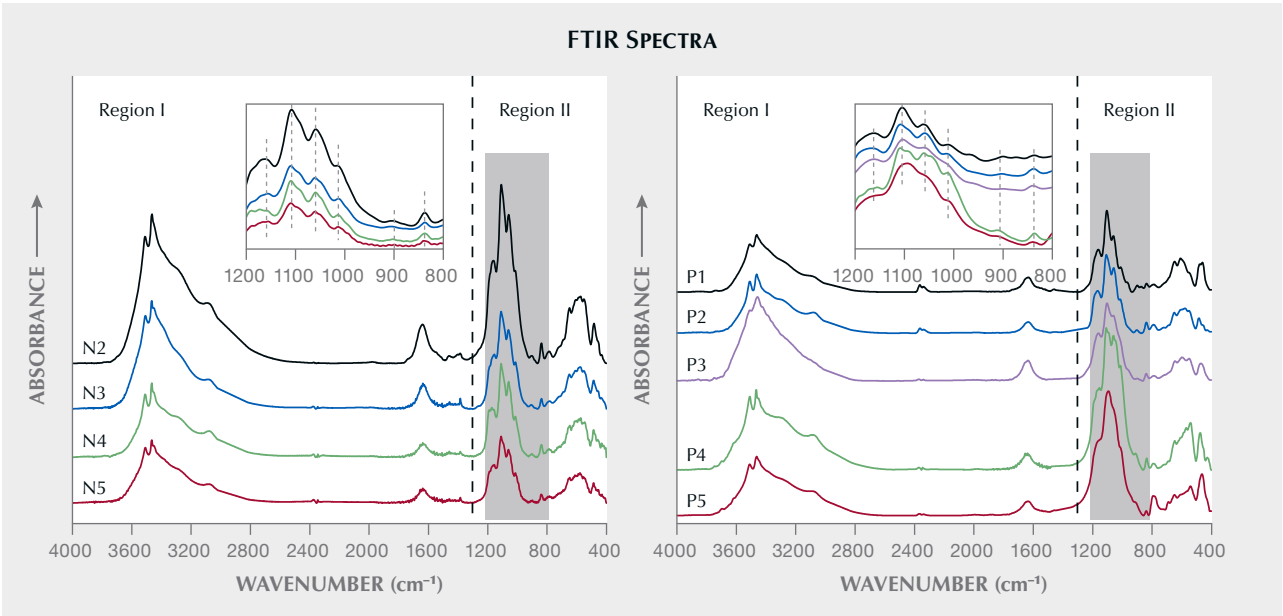

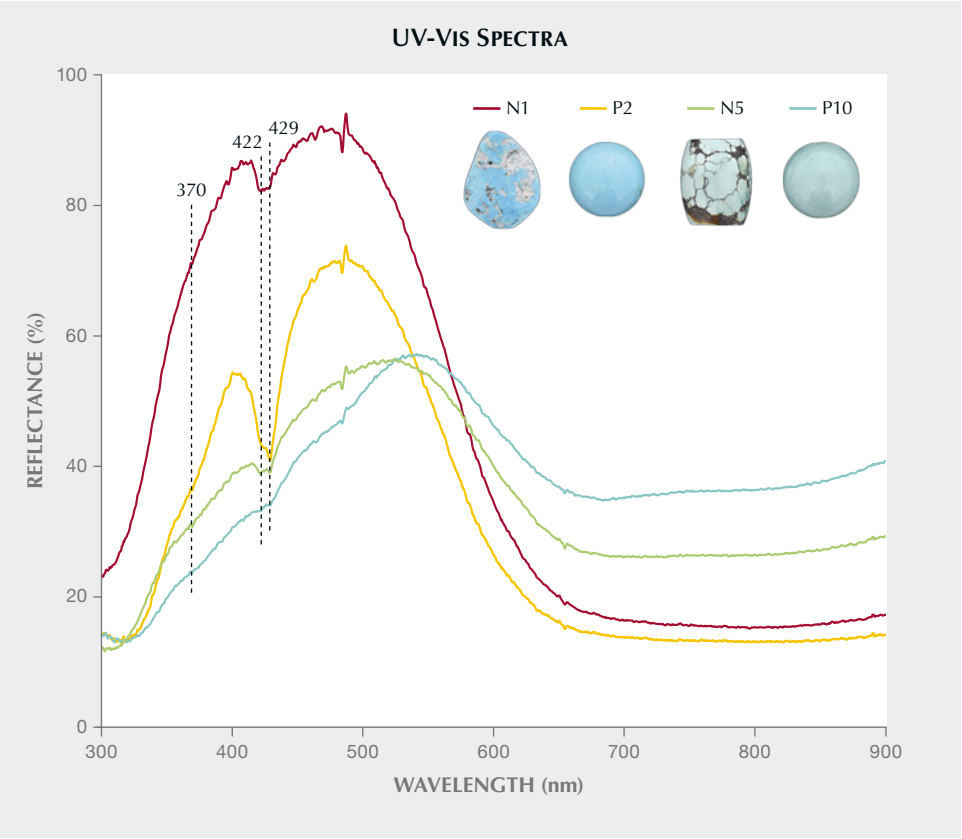

Figure 15. UV-Vis reflectance spectra of untreated (N1 and N5) and porcelain-treated (P2 and P10) turquoise samples. Their UV-Vis characteristics are essentially identical when comparing similar colors between treated and untreated.

absorption peak. It was difficult to distinguish the presence of Si-O-Si without careful comparison.

We detected no peaks of organic matter in the infrared spectrum, and the infrared absorption peak of Si-O was very similar to that of PO_4^{3-}.

UV-Vis Reflectance Spectrum Features. All the porcelain-treated and untreated specimens were measured with UV-Vis spectroscopy. In turquoise, copper is in a distorted octahedral coordination with six oxygens in an edge-sharing arrangement with pairs of alumina octahedra, and iron presumably replaces aluminum (Zhang et al., 1984; Foord and Taggart, 1998; Chen, 2009; Liu, 2019). The broad and strong absorption band near 620–750 nm is produced by the *d-d* electron transition of Cu^{2+}. The *d-d* electron transition of Fe^{3+} produces an absorption band near the violet region at 425 nm, while the weak absorption band in the ultraviolet region at 370 nm is caused by the Fe^{3+} electron transition and charge transferring from O^{2-} to Fe^{3+} (Foord and Taggart, 1998; Chen, 2009). The UV-Vis reflectance spectra of porcelain-treated turquoise (figure 15) show a broad absorption band in the yellow to red region (620–750 nm) and two absorption peaks in the purple region (~422 and 429 nm), which are almost identical to the UV-Vis absorption spectra of untreated turquoise. N5 and P10 are greener than N1 and P2 and have more iron, so their absorptions are stronger at 422 and 429 nm.

Basis for Identifying Porcelain-Treated Turquoise Using Nondestructive Methods. Both untreated and porcelain-treated turquoise can be identified through nondestructive testing, focusing on the appearance and composition characteristics of porcelain-treated turquoise (see the flowchart in figure 16):

1. the combination of strong surface luster and low density
2. fibrous filaments and potentially an area with greasy luster on the surface
3. high atomic ratio of iron to aluminum (>0.22) and low atomic percentage of phosphorus (<37.5%)
4. high silica content (>8.29 wt.%) in at least five test sites.

The silicon content at multiple test locations (without evidence of minerals that would account for it) is the decisive basis for identification of porcelain treatment, while the surface features and atomic

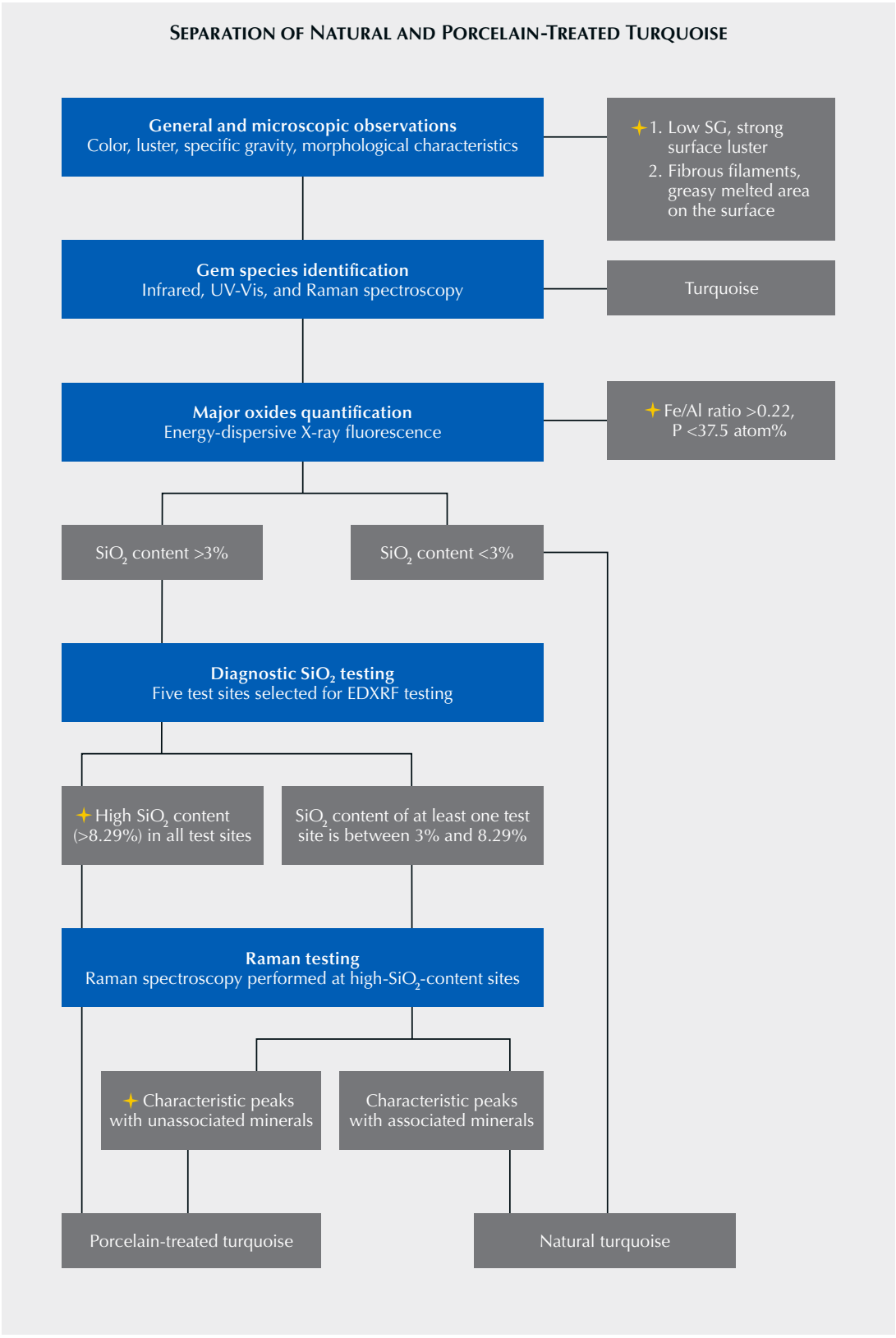

Figure 16. Identification flowchart for porcelain-treated turquoise. The blue boxes represent laboratory testing, while the gray boxes represent test results. The yellow stars indicate key distinguishing features.

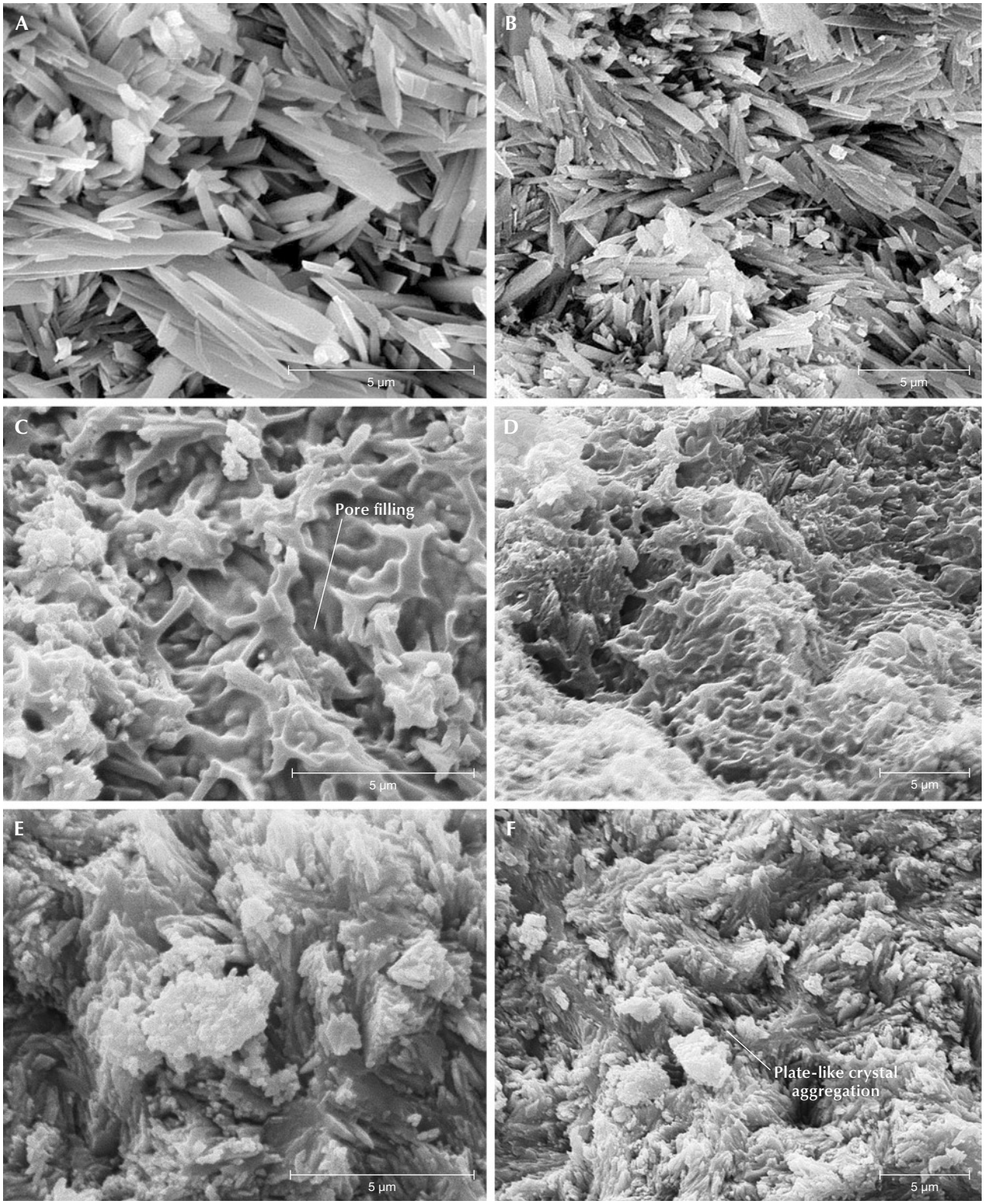

Figure 17. Morphological characteristics of untreated and porcelain-treated turquoise. The structure of untreated turquoise (N14) is shown via SEM imaging with 10,000× magnification (A) and 6,000× magnification (B). C and D: Microcrystal boundaries of porcelain-treated turquoise (H3) are blurred and pores are filled by colloidal material. E and F: The microcrystals inside sample H3 are columnar and plate-shaped.

content are the auxiliary basis. In the identification process, however, it is still necessary to comprehensively consider all four factors.

ESEM. Three porcelain-treated specimens with different densities (P4, H2, and H3) and one untreated specimen (N14) were examined with ESEM. Turquoise is triclinic and has a mostly cryptocrystalline structure with very large pores (Cid-Dresdner, 1965; Foord and Taggart, 1998; Chen, 2009; Abdu et al., 2011). Fine crystals can be observed under an electron microscope, mostly in the form of thin columns, plates, and scales. Figure 17 (A and B) shows the structure of untreated turquoise under 10,000× and 6,000× magnification, respectively. In specimens with different densities, there are also differences in the arrangements of microcrystals; turquoise with high density has a compact arrangement and small pores, whereas turquoise with low density has a loose, disorderly arrangement and large pores (Cid-Dresdner, 1965).

Three porcelain-treated specimens (P4, H2, and H3) were selected for SEM examination, and their structural characteristics were compared with those of untreated turquoise. For observation of each split specimen, three test positions were selected from edge to center. SEM images of porcelain-treated turquoise near the edge of the test sites are shown in figure 17 (C and D). Microcrystals within porcelain-treated turquoise lack the typical columnar and plate-like crystals of untreated turquoise aggregates. These microcrystals within porcelain-treated turquoise are approximately lath-shaped with a disorderly distribution, and they have rounded microcrystalline edges and blurred boundaries. Also, gel-like colloids (e.g., figure 17C) distributed between the pores of microcrystals and the crystal surface can be seen (the pores between crystals are no longer visible). As shown in figure 17 (E and F), the test location near the center was less affected by the porcelain treatment and the crystals are columnar and plate-shaped, with observable edges and pores.

The surface characteristics produced by porcelain treatment are obvious, while the effect within the stone is less evident, similar to the EDXRF results. SEM imaging shows that the morphology near the center of porcelain-treated turquoise is similar to that of untreated turquoise, with complete crystal shapes, obvious pores, and a disorderly arrangement of microcrystals. SEM is a useful technique to distinguish untreated from porcelain-treated turquoise through identification of microcrystal morphologies and colloid distributions. However, it is not suitable for routine gem identification because of its destructiveness.

CONCLUSIONS

Porcelain-treated turquoise can be reliably separated from natural turquoise if a certain combination of characteristics are present: low specific gravity, strong surface luster, surface features (including fibrous filaments, greasy melted areas, and color distribution), high silica content (>8.29 wt.%), a high atomic ratio of iron to aluminum (>0.22), a low atomic percentage of phosphorus (<37.5%), and evidence of colloid-filled pores with SEM examination. High silica content is the most diagnostic feature of porcelain treatment, while low SG combined with strong luster and high atomic ratio of iron to aluminum are auxiliary identification criteria. However, it is necessary to comprehensively evaluate all four factors to make a final determination. The infrared and UV-Vis absorption spectra characteristics are basically the same for untreated and porcelain-treated turquoise and therefore not useful for separation. SEM observation of surface micromorphology provides distinct evidence of porcelain treatment but requires coating with carbon or gold, making it unsuitable for routine identification.

ABOUT THE AUTHORS

Ms. Huang holds a bachelor's degree in gemology from the Gemmological Institute, China University of Geosciences (CUG) in Wuhan. Associate Professor Chen (corresponding author, chenquanli_0302@163.com), Professor Li (yanli@cug.edu.cn), and Professor Yin teach at the Gemmological Institute, CUG, where Mr. Gao and Mr. Du are master's students and Mr. Xu is a graduate student. Associate Professor Chen is teaching for two years (until May 2024) at the School of Jewelry, West Yunnan University of Applied Sciences.

ACKNOWLEDGMENTS

This work has been funded by Hubei Gem & Jewelry Engineering Technology Center (No. CIGTXM-03-202201). The project was also supported by the "CUG Scholar" Scientific Research Funds at China University of Geosciences (Wuhan) (No.2022185), NSFC funding (No. 41874105), Fundamental Research Funds for National University, CUG (No. CUGDCJJ202221), Philosophy and Social Science Foundation of Hubei Province (No. 21G007). The publication of this article in 2022 marks the 30th anniversary of the Gemmological Institute and the 70th anniversary of the China University of Geosciences in Wuhan.

REFERENCES

Abdu Y.A., Hull S.K., Fayek M., Hawthorne F.C. (2011) The turquoise-chalcosiderite Cu(Al, Fe^{3+})$_6$(PO$_4$)$_4$(OH)$_8$·4H$_2$O solid-solution series: A Mossbauer spectroscopy, XRD, EMPA, and FTIR study. *American Mineralogist*, Vol. 96, No. 10, pp. 1433–1442, http://dx.doi.org/10.2138/am.2011.3658

Beale T.W. (1973) Early trade in highland Iran: A view from a source area. *World Archaeology*, Vol. 5, No. 2, pp. 133–148, http://dx.doi.org/10.1080/00438243. 1973. 9979561

Čejka J., Sejkora J., Macek I., Malíková R., Wang L., Scholz R., Frost R.L. (2015) Raman and infrared spectroscopic study of turquoise minerals. *Spectrochimica Acta Part A: Molecular and Biomolecular Spectroscopy*, Vol. 149, pp. 173–182, http://dx.doi.org/10.1016/j.saa.2015.04.029

Chen Q.L. (2009) Study on recycling technology and mechanism of turquoise. PhD thesis, China University of Geosciences [in Chinese].

Chen Q.L., Qi L.J. (2007) Study on the vibrational spectra characters of water in turquoise from Ma'anshan. *Journal of Mineralogy and Petrology*, Vol. 27, No. 1, pp. 30–35, http://dx.doi.org/10.3969/j.issn.1001-6872.2007.01.006 [in Chinese].

Chen Q.L., Yuan X.Q., Chen J.Z., Zhou J.H. (2010a) Structural characteristics of turquoise filled with aluminum phosphate adhesive. *Earth Science-Journal of China University of Geosciences*, Vol. 35, No. 6, pp. 1023–1028, http://dx.doi.org/10.3799/dqkx.2010.115 [in Chinese].

Chen Q.L., Yuan X.Q., Chen J.Z., Qi L.J. (2010b) Study on the treatment of turquoise using Raman spectroscopy. *Spectroscopy and Spectral Analysis*, Vol. 30, No. 7, pp. 1789–1792 [in Chinese].

Chen Q.L., Yin Z.W., Qi L.J., Xiong Y. (2012) Turquoise from Zhushan County, Hubei Province, China. *G&G*, Vol. 48, No. 3, pp. 198–204, http://dx.doi.org/10.5741/GEMS.48.3.198

Choudhary G. (2010) A new type of composite turquoise. *G&G*, Vol. 46, No. 2, pp. 106–113, http://dx.doi.org/10.5741/GEMS.46.2.106

Cid-Dresdner H. (1965) Determination and refinement of the crystal structure of turquois, CuAl$_6$(PO$_4$)$_4$(OH)$_8$·4H$_2$O. *Zeitschrift für Kristallographie - Crystalline Materials*, Vol. 121, No. 1-6, pp. 113–87, http://dx.doi.org/10.1524/zkri.1965.121.16.87

Deng Q., Hu J.M., Wang X., Cao Y., Yang W. (2019) Study on identification of turquoise treated with "porcelain." *China International Jewelry Academic Exchange Conference Proceedings*, http://dx.doi.org/10.26914/c.cnkihy.2019.013579 [in Chinese].

Evans O.H., Southward J. (1914) A further note on the occurrence of turquoise at Indio Muerto, northern Chile. *Man*, Vol. 14, pp. 37–39, http://dx.doi.org/10.2307/2788948

Farmer V.C. (1974) *The Infrared Spectra of Minerals*. Mineralogical Society Monograph 4, London.

Foord E.E., Taggart J.E. (1998) A reexamination of the turquoise group: The mineral aheylite, planerite (redefined), turquoise and coeruleolactite. *Mineralogical Magazine*, Vol. 62, No. 1, pp. 93–111, http://dx.doi.org/10.1180/002646198547495

Fritsch E., Stockton C.M. (1987) Infrared spectroscopy in gem identification. *G&G*, Vol. 23, No. 1, pp. 18–26, http://dx.doi.org/10.5741/GEMS.23.1.18

Fritsch E., McClure S.F., Ostrooumov M., Andres Y., Moses T.M., Koivula J.I., Kammerling R.C. (1999) The identification of Zachery-treated turquoise. *G&G*, Vol. 31, No. 1, pp. 4–16, http://dx.doi.org/10.5741/GEMS.35.1.4

Harbottle G., Weigand P. (1992) Turquoise in Pre-Columbian America. *Scientific American*, Vol. 266, No. 2, pp. 78–85, http://www.jstor.org/stable/24938943.

He C., Cao F.F., Di J.R., Yang M.X., Lu R., Liu L. (2018) Interpretation of national standard "turquoise classification." *Journal of Gems and Gemmology*, Vol. 20, No. 6, pp. 7–17, http://dx.doi.org/10.15964/j.cnki.027jgg.2018.06.002 [in Chinese].

Hedquist S. (2016) Ritual practice and exchange in the late prehispanic Western Pueblo Region: Insights from the distribution and deposition of turquoise at Homol'ovi I. *KIVA*, Vol. 82, No. 3, pp. 209–231, http://dx.doi.org/10.1080/00231940.2016.1214056

Koivula J.I., Kammerling R.C., Fritsch E. (1992) Gem News: Modern-day turquoise oiling. *G&G*, Vol. 28, No. 2, p. 137.

Krishnamurti D. (1958) The Raman spectrum of quartz and its interpretation. *Proceedings of the Indian Academy of Sciences-Section A*, Vol. 47, No. 5, pp. 276–291, http://dx.doi.org/10.1007/BF03052811

Krishnan R. (1945) Raman spectrum of quartz. *Nature*, Vol. 155, p. 452, http://dx.doi.org/10.1038/155452a0

Lind T., Schmetzer K., Bank H. (1983) The identification of turquoise by infrared spectroscopy and X-ray powder diffraction. *G&G*, Vol. 19, No. 3, pp. 164–168, http://dx.doi.org/10.5741/GEMS.19.3.164

Liu L. (2019) Study on origin, factors and grading of the color of turquoise from China. Master's thesis, China University of Geosciences (Wuhan) [in Chinese].

Liu L., Yang M.X. (2018) Study on EDXRF method of turquoise composition. *Spectroscopy and Spectral Analysis*, Vol. 38, No. 6, pp. 1910–1916 [in Chinese].

Liu X.F., Lin C.L., Li D.D., Zhu L., Song S., Liu Y., Shen C.H. (2018) Study on mineralogy and spectroscopy of turquoises from Hami, Xinjiang. *Spectroscopy and Spectral Analysis*, Vol. 38, No. 4, pp. 1231–1239 [in Chinese].

Luan L.J., Han Z.X., Wang C.Y., Zhang Y.W. (2004) Elementary research on color-forming mechanism of turquoise. *Northwestern Geology*, Vol. 37, No. 3, pp. 77–82, http://dx.chinadoi.cn/10.3969/j.issn.1009-6248.2004.03.013 [in Chinese].

Luo Y.F., Yu X.Y., Zhou Y.G., Yang X.G. (2017) A study of texture and structure of turquoise from Luonan, Shaanxi Province. *Acta Petrologica et Mineralogica*, Vol. 36, No. 1, pp. 115–123, http://dx.doi.org/10.3969/j.issn.1000-6524.2017.01.012 [in Chinese].

Mansour A.M.A. (2014) *Turquoise in Ancient Egypt: Concept and Role*. British Archaeological Reports, Oxford, UK, http://dx.doi.org/10.30861/9781407312347

McClure S.F., Kane R.E., Sturman N. (2010) Gemstone enhancement and its detection in the 2000s. *G&G*, Vol. 46, No. 3, pp. 218–240, http://dx.doi.org/10.5741/GEMS.46.3.218

Ou W.C., Yue S.W., Gao K. (2016) Identification of turquoise and treated turquoise. *Journal of Gems and Gemmology*, Vol. 18, No. 1, pp. 6–14, http://dx.doi.org/10.3969/j.issn.1008-214X.2016.01.003 [in Chinese].

Ovissi M., Yazdi M., Ghorbani M. (2017) Turquoise; a gemstone that relates geology to archaeology and anthropology. *The First Symposium of Turquoise: Industry and Culture* [in Persian].

Pristacz H., Wildner M., Hammer V.M.F., Libowitzky E. (2013) Investigations of a synthetic turquoise. *Conference on Raman and Luminescence Spectroscopy in the Earth Sciences*, pp. 81–82, http://dx.doi.org/10.1007/978-3-540-72816-022301

Schwarzinger B., Schwarzinger C. (2017) Investigation of turquoise imitations and treatment with analytical pyrolysis and infrared spectroscopy. *Journal of Analytical and Applied Pyrolysis*, Vol. 125, pp. 24–31, http://dx.doi.org/10.1016/j.jaap.2017.05.002

Song J.W. (2008) On the influence and development of Chinese ancient porcelain to the world. *Journal of Taiyuan Urban Vocational College*, No. 11, pp. 141–142, http://dx.doi.org/10.3969/j.issn.1673-0046.2008.11.084 [in Chinese].

Štubňa J., Andrášiová A. (2021) Turquoise from Armenia. *Journal of Gemmology*, Vol. 37, No. 5, pp. 454–456.

Tu H.K. (1997) Metallogenic characteristics of turquoise in the eastern Qinling Mountains. *Nonmetallic Geology*, No. 3, pp. 24–25 [in Chinese].

Wang F. (1986) A gemological study of turquoise in China. *G&G*, Vol. 22, No. 1, pp. 35–37, http://dx.doi.org/10.5741/GEMS.22.1.35
Weigand P.C., Harbottle G., Sayre E.V. (1977) Turquoise sources and source analysis: Mesoamerica and the southwestern USA. In T.K. Earle and J.E. Ericson, Eds., *Exchange Systems in Prehistory*. Academic Press, New York, pp. 15–34, http://dx.doi.org/10.1016/B978-0-12-227650-7.50008-0
Xie H., Pei J.C., Xu Y. (2021) Gaspeite: A new gem material like turquoise. *Journal of Gems and Gemmology*, Vol. 12, No. 3, pp. 41–43, http://dx.doi.org/10.3969/j.issn.1008-214X.2010.03.009 [in Chinese].
Xu F.S., Chen Q.L., Ding W., Wang H.T. (2021) Study on fluorescence spectrometry of natural and organic filling treated turquoise. *Spectroscopy and Spectral Analysis*, Vol. 41, No. 9, pp. 2918–2923 [in Chinese].
Xu Y.F., Di J.R. (2018) Gemological identification of natural turquoise and treatment turquoise in Hubei. *Acta Petrologica et Mineralogica*, Vol. 37, No. 4, pp. 646–654, http://dx.doi.org/10.3969/j.issn.1000-6524.2018.04.010 [in Chinese].
Yang Y.Z., Zhang J.Z., Lan W.L., Cheng Z.J., Yuan Z.J., Zhu Z.F. (2017) 2013 excavation bulletin of Jiahu site, Wuyang County, Henan Province. *Archaeology*, No. 12, pp. 3–20 [in Chinese].
Zalinski E.R. (1907) Turquoise in the Burro Mountains, New Mexico. *Economic Geology*, Vol. 2, No. 5, pp. 464–492, http://dx.doi.org/10.2113/gsecongeo.2.5.464
Zhang H.F., Lin C.Y., Ma Z.W., Yang Z.G., Zhang E.L. (1984) Magnetic properties, characteristic spectra and colors of turquoise. *Geochemistry*, Vol. 3, pp. 322–332, http://dx.doi.org/10.1007/BF03179305
Zhou S.Q., Jiang F.J. (2005) The research of the turquoise in Xichuan of Henan. *Journal of Nanyang Teachers' College*, Vol. 4, No. 3, pp. 63–65, http://dx.doi.org/10.3969/j.issn.16716132.2005.03.019 [in Chinese].
Zhu H.W., Cheng Y.F., Shan G.Q. (2016) Identification of turquoise imitation. *Superhard Material Engineering*, Vol. 28, No. 6, pp. 58–60, https://doi.org/10.3969/j.issn.1673-1433.2016.06.021 [in Chinese].